BIOCHEMISTRY
including biophysical chemistry & molecular biology

Article

pubs.acs.org/biochemistry

Activation of 11*R*-Lipoxygenase Is Fully Ca^{2+}-Dependent and Controlled by the Phospholipid Composition of the Target Membrane

Reet Järving,[†] Aivar Lõokene,[†] Reet Kurg,[‡] Liina Siimon,[†] Ivar Järving,[†] and Nigulas Samel*,[†]

[†]Department of Chemistry, Tallinn University of Technology, Akadeemia tee 15, 12618 Tallinn, Estonia

[‡]Institute of Technology, University of Tartu, Nooruse St 1, 50411 Tartu, Estonia

ABSTRACT: Activation of some lipoxygenases (LOX) is found to be related to the selective membrane binding upon cell stimulation. In this study, a systematic analysis of the effect of the lipid composition on the membrane binding efficiency, Ca^{2+} affinity, and enzymatic activity of 11*R*-LOX was performed. The analysis of the membrane targeting by fluorometric and surface plasmon resonance measurements in the absence of Ca^{2+} showed an exclusive binding of 11*R*-LOX to the anionic phospholipids (phosphatidylinositol < phosphatidylglycerol ≈ phosphatidylserine) containing model membranes. The presence of Ca^{2+} enhanced the rate of interaction and influenced its mode. The modulation of the activity of 11*R*-LOX indicated that (i) Ca^{2+} binding is a prerequisite for productive membrane association, (ii) the reaction of 11*R*-LOX with arachidonic acid coincided with and was driven by its Ca^{2+}-mediated membrane association, and (iii) phosphatidylethanolamine and anionic phospholipids had a synergistic effect on the Ca^{2+} affinity, in line with a target-activated messenger affinity mechanism [Corbin, J. A., et al. (2007) *Biochemistry 46*, 4322−4336]. According to the mechanism proposed in this report, 11*R*-LOX can bind to the membranes in two different modes and the efficiency of productive membrane binding is determined by a concerted association of Ca^{2+} and lipid headgroups.

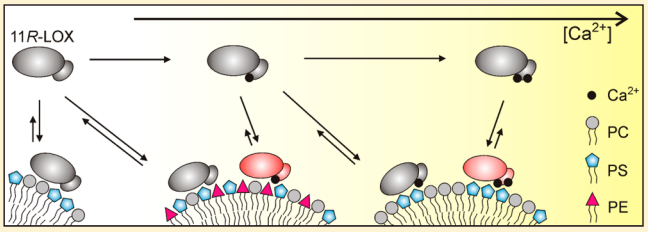

Lipoxygenases catalyze the stereospecific oxygenation of polyunsaturated fatty acids into the corresponding hydroperoxy acids and are classified with respect to their positional selectivity of incorporation of the molecular oxygen into arachidonic acid (AA).[1,2] Mammalian LOX are activated upon cell stimulation and cooperate with cytosolic phospholipase A_2 ($cPLA_2$) to generate eicosanoids that play significant roles in many pathophysiological processes.[3,4]

All LOX so far determined with the X-ray structure have a similar topology regardless of their source and size.[1,5] They consist of two domains, viz., a small N-terminal barrel-like regulatory domain and a larger, mostly helical, catalytic C-terminal domain. Jankun and co-workers suggest that LOX may possess a second regulatory subdomain, a PDZ-like fragment, in their catalytic portions.[6] The N-terminal domain consists of eight antiparallel β-strands and is named according to different classifying criteria a C2-like, LH2, or PLAT domain.[7,8] The N- and C-terminal domains are covalently interconnected by a randomly coiled oligopeptide. The N-terminal domain is not essential for catalytic activity but contacts the C-terminal domain via an interdomain contact plain and plays a significant role in the regulation of the turnover via Ca^{2+}-dependent membrane binding.[9−14] Ca^{2+} has been found to regulate the activity of human 5-LOX[15] and coral 8*R*-LOX.[16−18] *Plexaura homomalla* 8*R*-LOX contains three specific calcium-binding sites in its β-barrel domain.[19] These surface-exposed Ca^{2+}-binding residues correspond to those proposed for human 5-LOX[9] and might initiate the insertion of 8*R*-LOX into the phospholipid bilayer. Ca^{2+} also enhances the membrane binding of rabbit 12/15-LOX and soybean LOX-1, but specific Ca^{2+}-binding amino acids do not appear to be involved.[12,20]

The lipid composition of the membranes of different organelles may vary widely. In addition, the two monolayers that constitute a defined membrane bilayer may drastically differ in lipid composition.[21,22] Phosphatidylcholine (PC) and phosphatidylethanolamine (PE) are the most abundant phospholipids in eukaryotic cell membranes, constituting 30−50 and 20−50% of total phospholipids, respectively.[23,24] Phosphatidylserine (PS) and phosphatidylinositol (PI) are the most abundant negatively charged phospholipids in eukaryotic membranes. Phosphatidylglycerol (PG) is present in smaller amounts.[22] The Ca^{2+}-binding loops of the C2 domains are specialized to generate different types of protein−membrane interactions.[25−27] Many cytosolic proteins with the C2 domain are translocated to the plasma membrane (PM) during cell signaling and other cellular processes. PS, PI 4,5-bisphosphate, and PI 3,4,5-trisphosphate that are present in PM play important roles in their specific PM recruitment.[28] Previous studies with mammalian lipoxygenases conducted in various cell types have found that cytoplasmic Ca^{2+} signals drive 5-LOX primarily to the PC-rich nuclear membrane (NM).[10,29] Negatively charged lipids in PC vesicles at 10−20 mol %

Received: August 8, 2011
Revised: March 26, 2012
Published: March 26, 2012

inhibit the activity of 5-LOX by 20−60%.[30] 15-LOX-1 primarily targets the PM in human dendritic cells.[31]

Two different mechanisms have been proposed for a specific intracellular targeting arising from the coincident detection of a global second messenger (Ca^{2+} signal) and a localized target molecule (target lipids).[32] The messenger-activated-target-affinity (MATA) mechanism is characterized by a targeting protein that possesses an apo state with a high affinity for the second messenger and a low affinity for the target molecule. The target-activated-messenger-affinity (TAMA) mechanism is characterized by a targeting protein that possesses an apo state with a low affinity for the second messenger as well as a low affinity for the target. By this mechanism, both the messenger and the target have to be simultaneously present to allow the protein to interact with them under physiological conditions. The TAMA mechanism could be further enhanced by positive cooperativity in the binding of two or more specific target molecules (lipids) as is described for protein kinase C, synaptotagmin 1, and rabphilin-3A.[33−35]

The arachidonate 11*R*-LOX from the Arctic soft coral *Gersemia fruticosa* binds reversibly to *Escherichia coli* membranes in the presence of millimolar Ca^{2+} concentrations.[36] Furthermore, the presence of calcium ions and cellular membranes is a prerequisite for the catalytic activity of this enzyme. As is evident from the sequence alignment,[36] all the Ca^{2+}-ligating residues found in *P. homomalla* 8*R*-LOX and proposed for human 5-LOX are conserved in 11*R*-LOX, indicating a possible similarity of the calcium activation of these enzymes. On the other hand, the surface-exposed tryptophans, which are involved in the membrane association of 5-LOX[29] and 8*R*-LOX, are not present in the putative membrane insertion loops of 11*R*-LOX, suggesting significant differences in the membrane insertion of the enzyme.

This work was designed as an the experimental control of our hypothesis that 11*R*-LOX can bind to the lipid membranes in different modes and that productive binding is determined by simultaneous action of Ca^{2+} and specific lipids. Using FRET and surface plasmon resonance (SPR), we monitored intrafacial binding and kinetics of interaction between 11*R*-LOX and model membranes of various lipid compositions in the absence and presence of Ca^{2+}. As a result, we propose a mechanism of membrane targeting and Ca^{2+}-dependent activation of 11*R*-LOX.

EXPERIMENTAL PROCEDURES

Overexpression and Purification of 11*R*-Lipoxygenase. *G. fruticosa* 11*R*-LOX was expressed with an N-terminal His_4 tag in BL21(DE3) cells (Novagen).[36] Following the induction of isopropyl β-D-thiogalactopyranoside at an A_{600} of 0.8, the cells were grown for 18 h at 10 °C, harvested, washed with 50 mM Tris-HCl (pH 8.0), and frozen at −80 °C. The frozen cells were resuspended in 20 mM Tris-HCl (pH 8.0) containing 1 mM phenylmethanesulfonyl fluoride (PMSF) and 1 mg/mL lysozyme and kept on ice for 30 min. The spheroplasts were sonicated for 10 × 5 s by using a Sonopuls HD 2200 ultrasonic homogenizer (Bandelin) at a power of 40−50%. The cell debris was removed by centrifugation at 100000*g* for 1 h at 4 °C. NaCl and imidazole at final concentrations of 300 and 10 mM, respectively, were added to the supernatant before incubation with an equilibrated nickel-nitrilotriacetic acid-agarose (Ni-NTA, Invitrogen) for 1 h at 4 °C. The supernatant/Ni-NTA mixture was loaded into the column and washed with the equilibration buffer [20 mM Tris-HCl (pH 8.0), 300 mM NaCl, and 10 mM imidazole]. The nonspecific bound proteins were eluted with 20 mM imidazole in the same buffer. After elution of 11*R*-LOX with 200 mM imidazole, the 10-fold diluted fractions were further purified by ion-exchange chromatography using a DEAE-Toyopearl 650 M resin (Toyo Soda Mfg. Co., Ltd.). The column was equilibrated and washed with 20 mM Tris-HCl (pH 8.0). Upon elution with a NaCl gradient, 11*R*-LOX was obtained at 150 mM. With these two-step purification procedures, the enzyme reached the electrophoretic homogeneity determined by sodium dodecyl sulfate−polyacrylamide gel electrophoresis (SDS−PAGE) and Coomassie Blue staining.

The purified enzyme was quantified from the protein band intensities of aliquots on a Coomassie-stained SDS−PAGE gel in comparison to the band intensities of a series of albumin standards run on the same gel. Approximately 12 mg of the purified 11*R*-LOX was obtained from a 1 L culture.

Preparation of Small Unilamellar Vesicles. Lipid vesicles were generated by mixing chloroform solutions of L-α-phosphatidylcholine (egg, chicken), L-α-phosphatidylethanolamine (transphosphatidylated, egg, chicken), L-α-phosphatidylinositol (liver, bovine), L-α-phosphatidyl-DL-glycerol (egg, chicken), L-α-phosphatidylserine (brain, porcine), cholesterol (Ch) (ovine wool), and 1,2-dioleyl-*sn*-glycero-3-phospho-L-serine-*N*-(5-dimethylamino-1-naphthalenesulfonyl) (dPS) (Avanti Polar Lipids) in the desired proportions. Lipids were dried from the organic solvent under a stream of nitrogen, and the last traces of the organic solvent were removed under vacuum for at least 1 h. The dried phospholipids were dissolved in 50 mM Tris-HCl (pH 8.0) and 100 mM NaCl for 1 h, vigorously vortex mixed for 2 min, and then subjected to direct probe sonication (15 × 5 s, an Ultrasonic cell disruptor, Cole Parmer, at a setting of 5) to produce small unilamellar vesicles (SUV). Following sonication, the insoluble material was removed from all lipid mixtures by centrifugation at 13000*g* for 15 min.

UV Spectroscopic Measurements. Lipoxygenase rates were determined by following the formation of the conjugated diene product at 236 nm (ε = 27000 M^{-1} cm^{-1}) with a Cary 50 Bio spectrophotometer (Varian). All the reaction mixtures had volumes of 1 mL and were constantly stirred using a magnetic stir bar at 20 °C. The assays were conducted in the presence of SUV, in 50 mM Tris-HCl (pH 8.0) and 100 mM NaCl at an AA concentration of 30 μM and $CaCl_2$ concentrations ranging from 0.05 to 3.0 mM unless otherwise described. The reactions were initiated by addition of enzyme (6.4 nM). The initial acceleration phase (the lag phase) of accumulation of the product at low concentrations of SUV or $CaCl_2$ (Figure 1A) was described well by an exponential growth equation (eq 1), giving the activation rate constant k_{act} of the enzyme. The steady-state velocity V of 11*R*-LOX was calculated from the linear slope of the time dependence of absorbance at 236 nm, $\Delta A/\Delta t$, due to the 11*R*-HpETE production (eq 2) at each concentration of SUV and $CaCl_2$.

$$A = A_s + A_0\, e^{k_{act}t} \quad (1)$$

$$V = \frac{\Delta A}{\Delta t} \times \varepsilon_{HpETE} \times C_{LOX} \times 60 \quad (2)$$

where A_s represents the offset of absorbance due to addition of substrate, A_0 is the absorbance value at time zero, and C_{LOX} represents the enzyme concentration. Time t is expressed in minutes; V is expressed in inverse seconds.

dx.doi.org/10.1021/bi201690z | *Biochemistry* 2012, 51, 3310−3320

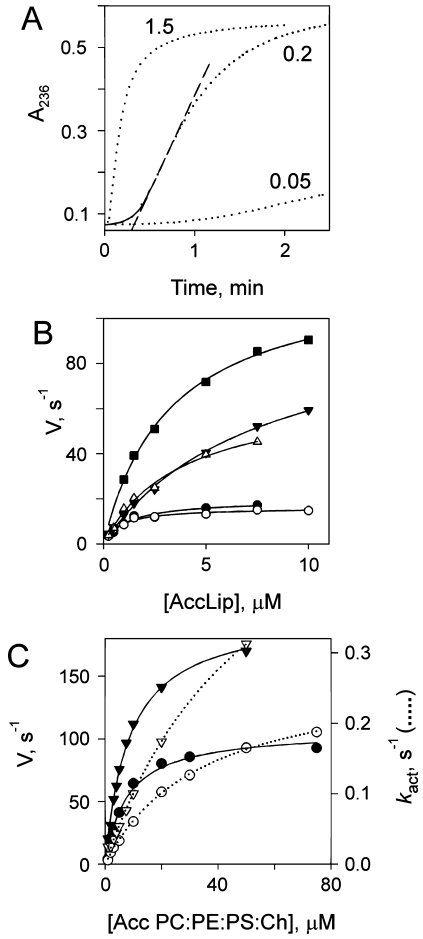

Figure 1. Phospholipid requirement of 11*R*-LOX activity. (A) Shown are 11*R*-LOX reaction progress curves (···) with AA (30 μM) monitored in a UV spectrophotometer cuvette at 236 nm in the presence of 0.05, 0.2, or 1.5 mM $CaCl_2$ and 50 μM PC/PE/PS/Ch vesicles (20:30:30:20). The initial lag phase of the product accumulation (solid part of the curve) fit well to the exponential growth equation (eq 1), giving the activation rate constant k_{act} of the enzyme. The steady-state activity V was calculated from the linear slope of the time dependence of A_{236} (−−−) using eq 2. (B) Effect of the composition of lipid mixtures on the activity of 11*R*-LOX in the presence of 1 mM $CaCl_2$. The vesicles consisted of PC and Ch (80:20) (●), PC (100%) (○), PC, PS, and Ch (50:30:20) (△), PC, PE, and Ch (50:30:20) (▼), or PC, PE, PS, and Ch (20:30:30:20) (■). (C) Interrelationship between V (black symbols, solid curves) and *k*act (white symbols, dotted curves) of 11*R*-LOX at 0.4 (● and ○) and 1 mM $CaCl_2$ (▼ and ▽). Experimental conditions: 50 mM Tris-HCl (pH 8.0), 100 mM NaCl, and 30 μM AA at 20 °C. The reaction was started by addition of 11*R*-LOX (5.0 nM). The curves in panels B and C represent the best fits to eq 3.

The plots of the catalytic activity of 11*R*-LOX versus accessible phospholipid (AccLip) or $CaCl_2$ concentration were subjected to a nonlinear least-squares analysis using either a single-independent site equation (eq 3) or the Hill equation (eq 4). In particular, all lipid titrations were analyzed by the single-independent site equation (eq 3), while Ca^{2+} titrations exhibited positive cooperativity and were thus analyzed by the Hill equation (eq 4):

$$Y = Y_{max}[x/(K_d + x)] \quad (3)$$

$$Y = Y_{max}[x^H/([Ca^{2+}]_{1/2}{}^H + x^H)] \quad (4)$$

where Y_{max} represents the apparent maximal activity (V_{max}) of 11*R*-LOX, x represents either the phospholipid concentration corrected for the leaflet (for phospholipid titrations) or the free Ca^{2+} concentration (for Ca^{2+} titrations), K_d represents the macroscopic equilibrium dissociation constant for lipid binding, and $[Ca^{2+}]_{1/2}$ represents the Ca^{2+} concentration that yields the half-maximal velocity. H is the Hill coefficient.

Fluorescence Spectroscopy. The experiments were conducted on a RF-5301PC spectrofluorophotometer (Shimadzu) at 20 °C and by continuous stirring in a standard assay buffer composed of 50 mM Tris-HCl (pH 8.0) and 100 mM NaCl. The excitation and emission slit widths were both 3 nm for all measurements.

Measurement of Equilibrium Ca^{2+}-Dependent Protein-to-Membrane FRET. The affinity of 11*R*-LOX for SUV was determined by monitoring the increase in the magnitude of the dansyl emission signal and the decrease in Trp fluorescence upon addition of Ca^{2+} to the solutions of 11*R*-LOX and SUV into which dPS was incorporated at 5 mol %. The enzyme (250 nM) and SUV (100 μM total lipids = 50 μM AccLip, except where indicated otherwise) were mixed in 3 mL of standard assay buffer. A small volume of the concentrated $CaCl_2$ stock solution was titrated into the SUV/protein mixture, by continuous stirring, to yield a total Ca^{2+} concentration of 0.05−2.0 mM. Parallel control experiments were performed using the same volume of water to titrate the SUV/protein mixture. After each addition, the sample was equilibrated for 3−10 min and fluorescence emission spectra were scanned (excitation wavelength of 280 nm and emission wavelength of 315−550 nm). Following the correction for dilution, the difference $\Delta Em_{517}(\pm Ca^{2+})/Em_{517}(-Ca^{2+})$ was plotted as a function of the total Ca^{2+} concentration, and the best fit was obtained using the Hill equation (eq 4), where Y_{max} represents the calculated maximal fluorescence change ΔEm_{max}, H represents the Hill coefficient, and $[Ca^{2+}]_{1/2}$ represents the Ca^{2+} concentration that induces a half-maximal fluorescence change.

Real-Time FRET Measurements of the Association Kinetics. To determine the observed rate constants for membrane association (k_{obs}) and the fluorescence amplitudes at equilibrium (ΔEm_{eq}), particular vesicles containing a small mole fraction of dansyl-PS were premixed with 0.1 mM EDTA or 0.4 mM $CaCl_2$ in standard assay buffer and allowed to equilibrate for 10 min. FRET was assessed by mixing 11*R*-LOX with the vesicles. 11*R*-LOX was excited, and the fluorescence emission of dPS was monitored (λ_{ex} = 280 nm; λ_{em} = 517 nm). The resulting time course yielded an increasing level of protein-to-membrane FRET with time and was subjected to a nonlinear least-squares best-fit analysis using a single- or double-exponential function (eq 5 or 6, respectively).

$$Y = \Delta Y_{eq}[1 - e^{-k_{obs}(t-t_0)}] + Y_0 \quad (5)$$

$$Y = \Delta Y_{eq1}[1 - e^{-k_{obs1}(t-t_0)}] + \Delta Y_{eq2}[1 - e^{-k_{obs2}(t-t_0)}] + Y_0 \quad (6)$$

where k_{obs} represents the observed rate constant for membrane association, Y represents the emission intensity Em at time t, Y_0 represents Em at the start of the data fit (Em_0), and ΔY_{eq} represents the fluorescence amplitude at equilibrium ($\Delta Em_{eq} = Em_{eq} - Em_0$).

SPR Measurements. The kinetics of the 11*R*-LOX−lipid interaction was investigated using an SPR system, Biacore 3000

(GE Healthcare Europe, Freiburg, Germany). The experiments were conducted with an L1 sensorchip at 25 °C. Liposomes (lipid concentration of 1 mM) were immobilized onto the sensorchip in the buffer that consisted of 50 mM Tris-HCl (pH 8.0) and 100 mM NaCl at a slow flow rate of 2 μL/min. The increases in response values after immobilization varied as follows: 4800−5000 RU (response units) for PC, 2600−3000 RU for the PC/PS mixture, 2700−3700 RU for the PC/PE/PS mixture, and 3600−4600 RU for the PC/PE/PS/Ch mixture. Loosely bound liposomes were removed by injection of 10 μL of 50 mM NaOH. The binding sites not occupied by the liposomes were blocked by injection of 20 μL of 0.1 mg/mL bovine serum albumin. Before binding experiments, 11*R*-LOX was dialyzed overnight against running buffer [50 mM Tris-HCl (pH 8.0), 100 mM NaCl, and 0.1 mM EDTA]. After dialysis, the concentration of 11*R*-LOX was determined. The binding of LOX to the immobilized liposomes was studied via single-cycle kinetics, increasing the concentration of the enzyme from 20 to 1000 nM. This was done in the presence of 0.1 mM EDTA or $CaCl_2$ at a concentration of 0.4, 1, or 2 mM. The surface was regenerated via repeated injections of 40 mM octyl β-D-glucopyranoside and 20 mM CHAPS and 10 s impulses of a 50 mM NaOH/2-propanol mixture (6:4, v/v). The sensorgrams were analyzed using Biacore evaluation version 4.0.1. It was assumed that the *R* of LOX (R_{LOX}) and the response of immobilized liposomes ($R_{ImmobLip}$) were directly proportional to the bound mass of 11*R*-LOX and SUV, respectively, and that the response of SUV was not dependent on lipid composition. To compare the response values of different experiments, normalization (norm*R*) was done by dividing R_{LOX} by $R_{ImmobLip}$. The association phase data were then fit to eq 6 by using SigmaPlot version 10. In this case, *Y* is the normalized response (norm*R*) of the biosensor at time *t*, Y_0 is the normalized response at the start of the data fit (normR_i), k_{obs1} and k_{obs2} are the observed rate constants for formation of two complexes between 11*R*-LOX and SUV, and ΔY_{eq1} and ΔY_{eq2} are the normalized responses at equilibrium (normΔR_{eq1} = normR_{eq1} − normR_i; normΔR_{eq2} = normR_{eq2} − normR_i). The normalized responses at equilibrium were summarized [normR_{eq}(sum) = normR_i + normΔR_{eq1} + normΔR_{eq2}] and plotted versus injected protein concentration. The normR_{max} (sum) and K_d(sum) were determined by a nonlinear least-squares analysis of the binding isotherm using eq 7:

$$\text{norm}R_{eq}(\text{sum}) = \frac{\text{norm}R_{max}(\text{sum}) \times C}{K_d(\text{sum}) + C} \quad (7)$$

where normR_{max} is the theoretical value of the response in the association of 11*R*-LOX with all immobilized vesicles and *C* is the concentration of 11*R*-LOX. The number of phospholipids involved in the binding of one 11*R*-LOX or stoichiometry (*n*) was calculated using eq 8:

$$n(\text{AccLip}/11R\text{-LOX}) = \frac{\text{MW}_{LOX}}{2 \times \text{norm}R_{max} \times \text{avMW}_{PL}} \quad (8)$$

where MW_{LOX} is the molecular weight of 11*R*-LOX and $avMW_{PL}$ is the average molecular weight of phospholipids of the particular liposome [e.g., for the PC/PE/PS/Ch (2:3:3:2) liposome, $avMW_{PL}$ = 0.2 × MW_{PC}+ 0.3 × MW_{PE} + 0.3 × MW_{PS} + 0.2 × MW_{Ch}].

RESULTS

The oxygenation of polyunsaturated fatty acids by lipoxygenases is associated with an activation step during which the resting ferrous enzyme is converted to an active ferric form by reaction with fatty acid hydroperoxide.[37,38] The activation process and/or catalytic reaction is inefficient when LOX has limited access to activating fatty acid hydroperoxides or substrates (fatty acid and O_2).[38,39] In the case of 11*R*-LOX, our previous studies showed that both Ca^{2+} and the membrane fraction are prerequisites for its catalytic activity.[36] The velocity of 11*R*-LOX, monitored by the formation of the conjugated diene product at 236 nm in the presence of Ca^{2+} and membranes, accelerates from zero to a maximal value and then continuously declines back to zero, with exhaustion of the substrate (Figure 1A). As the acceleration period can be completely abolished by the presence of a sufficient amount of SUV and Ca^{2+}, the lag phase does not result from an insufficient amount of activating hydroperoxides, but rather from the lack of accessibility of hydroperoxides and/or substrates when the enzyme is not membrane-associated. We presume that the initial acceleration in the LOX reaction reflects activation due to Ca^{2+}-mediated membrane binding. The induction period is shorter (a larger k_{act}) and the steady-state velocity higher at higher concentrations of liposomes and Ca^{2+}. Our preliminary results with purified 11*R*-LOX and vesicles whose lipid headgroup compositions mimic those of PM (12:35:22:9:22 PC:PE:PS:PI:Ch) and NM (61:21:4:7:7 PC:PE:PS:PI:Ch) showed a clear preference of 11*R*-LOX for the PM mimetic than for the NM mimetic, i.e., the higher reaction rate at a lower concentration of liposomes and Ca^{2+} when liposomes contained less PC and more PE, PS, and Ch. The contribution of 5 mol % phosphoinositides, including PI 4-phosphate, PI (3,4)-bisphosphate, PI (3,5)-bisphosphate, PI (4,5)-bisphosphate, or PI (3,4,5)-trisphosphate, to PM did not reveal major differences when compared with the PM alone (data not shown). In this work, we studied the effect of membrane lipids on 11*R*-LOX activity and the calcium binding affinity of 11*R*-LOX in the presence of membranes by using a set of lipids with different polar headgroups, including two neutral/zwitterionic glycerophospholipids (PC and PE), three anionic glycerophospholipids (PS, PG, and PI), and a steroid (Ch). In most cases, we used PC as a host lipid in the membranes of small unilamellar vesicles and added different guest lipids (30 mol %) because PC is an abundant lipid in animal cell membranes, and fractions of individual lipids other than PC and PE are moderate.

Modulation of 11*R*-LOX Activity by Membrane Lipids.

At low concentrations, lipids were tested as a mixture with PC and Ch (20 mol %). As shown in Figure 1B, membranes containing only PC or PC and Ch have a modest stimulatory effect on 11*R*-LOX activity. The steady-state V_{max} of 11*R*-LOX increases 3.5-fold in the presence of vesicles containing 30 mol % anionic lipid PS. Interestingly, substitution of a primary amino group for the trimethylammonium group of PC (i.e., replacement of 30 mol % PC with PE) causes a 5-fold increase in 11*R*-LOX activity. The addition of 30 mol % PS to the PC/PE/Ch vesicles resulted in a further increase in 11*R*-LOX activity and an ∼2-fold increase in binding affinity (i.e., decrease in the apparent K_d). Incorporation of 20 mol % cholesterol into membranes did not significantly alter the activation rate and catalytic activity of 11*R*-LOX (all data not shown).

dx.doi.org/10.1021/bi201690z | *Biochemistry* 2012, 51, 3310−3320

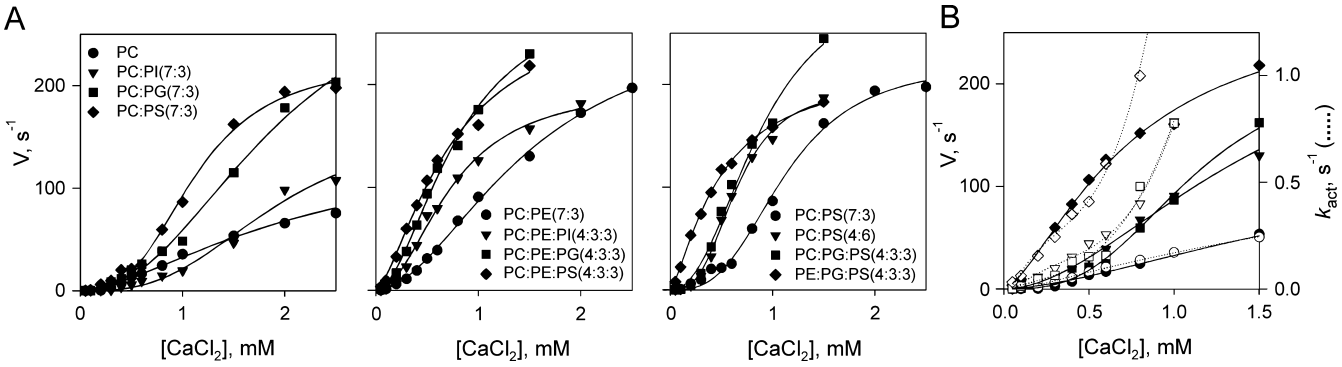

Figure 2. Ca^{2+} requirement of 11*R*-LOX activity in the presence of vesicles with various phospholipid compositions. (A) Plot of the steady-state velocity *V* of 11*R*-LOX (6.4 nM) vs $CaCl_2$ concentration in the presence of 50 μM accessible lipid. Solid curves represent the best fits to the Hill equation (eq 4), yielding the apparent V_{max} and $[Ca^{2+}]_{1/2}$ values and Hill coefficients summarized in Table 1. (B) Interrelationship between *V* (closed symbols, solid curves) and k_{act} (open symbols, dotted curves) of 11*R*-LOX. Shown are data for PC (● and ○), PC/PE (7:3) (▼ and ▽), PC/PS (7:3) (■ and □), and PC/PE/PS (4:3:3) (◆ and ◇) vesicles (50 μM accessible lipid). Experimental conditions: 50 mM Tris-HCl (pH 8.0), 100 mM NaCl, and 30 μM AA at 20 °C. The reaction was started by addition of 11*R*-LOX (6.4 nM).

Table 1. Comparison of Parameters Characterizing the Ca^{2+} Requirement of 11*R*-LOX Activity in the Presence of Various Phospholipid Vesicles

lipid mixture (molar ratio)	apparent V_{max} (s^{-1})	$[Ca^{2+}]_{1/2}$ (mM)	Hill coefficient	apparent $V_{max}/[Ca^{2+}]_{1/2}$ (s^{-1} mM^{-1})
PC	143 ± 25	2.12 ± 0.48	1.61 ± 0.18	70 ± 19
PC/PE (7:3)	270 ± 16	1.49 ± 0.11	1.88 ± 0.10	180 ± 17
PC/PI (7:3)	164 ± 20	1.90 ± 0.20	2.94 ± 0.40	90 ± 14
PC/PG (7:3)	323 ± 54	1.92 ± 0.30	2.29 ± 0.25	170 ± 38
PC/PS (7:3)	222 ± 11	1.12 ± 0.06	2.99 ± 0.28	200 ± 14
PC/PS (4:6)	197 ± 9	0.65 ± 0.03	3.00 ± 0.27	300 ± 20
PC/PG/PS (4:3:3)	316 ± 44	0.90 ± 0.13	2.21 ± 0.31	350 ± 70
PE/PG/PS (4:3:3)	221 ± 9	0.49 ± 0.03	1.36 ± 0.07	450 ± 33
PC/PE/PI (4:3:3)	199 ± 11	0.73 ± 0.05	2.03 ± 0.19	270 ± 24
PC/PE/PG (4:3:3)	297 ± 27	0.80 ± 0.09	1.85 ± 0.17	370 ± 54
PC/PE/PS (4:3:3)	286 ± 34	0.74 ± 0.14	1.49 ± 0.18	390 ± 86
PC/PE/PG/PS (3:4:1:2)	242 ± 8	0.67 ± 0.04	1.61 ± 0.08	360 ± 25
PC/PE/PG/PS/Ch (1:4:1:2:2)	235 ± 14	0.50 ± 0.05	1.44 ± 0.12	470 ± 55

As mentioned above, in some cases, the reaction of 11*R*-LOX exhibits a pronounced lag phase during which the enzyme is activated. As shown in Figure 1C, the duration of the lag phase depends on the concentration of liposomes as well as that of Ca^{2+}. At higher liposome concentrations, only the duration of the lag phase, not the steady-state velocity of 11*R*-LOX, was affected. The increase in the Ca^{2+} concentration significantly increased the activation rate of 11*R*-LOX. At Ca^{2+} concentrations of <1 mM, the activity of 11*R*-LOX remained lower even at a sufficient amount of SUV pointing to the low Ca^{2+} binding affinity of 11*R*-LOX.

Calcium Dependence of 11*R*-LOX Activity in the Presence of Model Membranes. Our previous study showed that for maximal dioxygenase activity the crude preparation of 11*R*-LOX required the addition of 10 mM $CaCl_2$ to the reaction medium.[36] The latter preliminary results with PM and NM mimetics indicated that there was a strong synergism between the phospholipid composition of vesicles and the calcium concentration required for the activity of 11*R*-LOX.

While the calcium concentration required for the activation and catalytic activity of 11*R*-LOX is strongly dependent on the content of phospholipids of the phospholipid bilayer, the steady-state reaction rates of 11*R*-LOX with AA in the presence of various SUV were plotted versus the free Ca^{2+} concentration and fit best to the Hill model as illustrated in Figure 2A. To characterize different liposomes, $V_{max}/[Ca^{2+}]_{1/2}$ was used (Table 1). The data show that anionic phospholipids (anPL) in PC vesicles improve the enzyme catalytic ability to different degrees in the following order: PI < PG < PS. Not only the headgroup charge but also the molecular structure of lipids is an important factor in the ability of Ca^{2+} to activate 11*R*-LOX. For example, an increase of the amount of the fraction of PS (from 30 to 60%) in PC vesicles causes a 1.7-fold increase in the calcium binding affinity (lower $[Ca^{2+}]_{1/2}$), but not significant changes in the maximal velocity of 11*R*-LOX. The replacement of a part of PS with PG [e.g., PC:PS (4:6) vs PC:PG:PS (4:3:3)] results in similar calcium binding affinities but increased the catalytic activity of 11*R*-LOX.

Further analysis of Figure 2 and the data listed in Table 1 indicates that the substitution of PE for 30% PC causes a decrease in $[Ca^{2+}]_{1/2}$, resulting in an increase in the catalytic activity of 11*R*-LOX at lower calcium concentrations and a 2–3-fold increase in $V_{max}/[Ca^{2+}]_{1/2}$. The best-fit Hill coefficient values of 1.4–3.0 (Table 1) suggest that the catalytic activity of 11*R*-LOX is driven by the binding of multiple Ca^{2+} ions with positive cooperativity, and the composition of the membrane has a significant effect on the Ca^{2+} binding of 11*R*-LOX. The decrease of the Hill coefficients, when PE is added to the PC/anPL membrane, may point to the participation of PE in the coordination of Ca^{2+} in the calcium-binding site of 11*R*-LOX.

dx.doi.org/10.1021/bi201690z | *Biochemistry* 2012, 51, 3310–3320

As shown in Figure 2B, the duration of the lag phase of the 11*R*-LOX reaction depends on the concentration of Ca^{2+}. At a low concentration of Ca^{2+} (<0.5 mM), an increase linearly increases both the activation rate constant and the steady-state velocity of 11*R*-LOX. At higher Ca^{2+} concentrations, there is an exponential decrease in the lag phase and this induction period can be completely abolished by the presence of a sufficient amount of Ca^{2+}. The latter depends on the composition of liposomes and is lower for the PC/PE/anPL liposome.

Taken together, for activation, 11*R*-LOX needs the presence of both Ca^{2+} and liposomes. The concentration of Ca^{2+} necessary for activation depends on the composition of the liposomes, indicating the coincident detection of multiple signals, Ca^{2+} and one or more target lipids.

Equilibrium Ca^{2+} Dependence of Targeting of 11*R*-LOX to Membranes. To investigate the relationship between 11*R*-LOX membrane binding and the appearance of activity, we monitored the Ca^{2+}-dependent membrane targeting of 11*R*-LOX by FRET.

First, to determine the Ca^{2+} binding affinity of 11*R*-LOX in the absence of membranes, the intrinsic tryptophan fluorescence of 11*R*-LOX was tested in the absence or presence of $CaCl_2$. No changes were found in the fluorescence emission spectra of 11*R*-LOX upon addition of Ca^{2+} (data not shown), indicating that the binding of Ca^{2+} ions does not generate detectable environmental changes of 11*R*-LOX tryptophans. The Ca^{2+} binding affinity in the presence of membranes was measured by quantitating FRET between intrinsic tryptophan donors in 11*R*-LOX and acceptor dansyl fluorophores in SUV (Figure 3). The energy transfer is dependent on the proximity

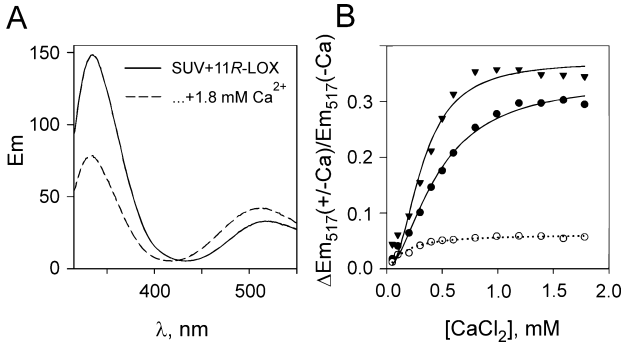

Figure 3. Equilibrium binding of 11*R*-LOX to model membranes. Membrane docking was quantitated by measuring the protein-to-membrane FRET between native Trp donors in the protein and dPS acceptor in SUV. (A) Fluorescence emission spectra in the presence of dPS-containing liposomes. Membrane binding is indicated by the reduction in Trp fluorescence (334 nm) accompanied by an increase in dansyl fluorescence (517 nm). (B) Ca^{2+}-dependent equilibrium binding of 11*R*-LOX to phospholipid vesicles. Shown are Ca^{2+} titration curves for the Ca^{2+}-triggered docking of 11*R*-LOX to SUV composed of PC, PE, PS, and dPS (40:30:25:5) (●) or PC, PE, PS, dPS, and Ch (20:30:25:5:20) (▼). Empty circles (○) correspond to data from the control experiment in the absence of Ca^{2+}. Solid curves represent the best fits to the Hill equation.

of donor and acceptor molecules and will occur only when the protein is bound to the membrane (Figure 3A). The resulting protein-to-membrane FRET data were plotted against the added Ca^{2+} concentration and fit best to the Hill model with $[CaCl_2]_{1/2}$ values of 0.46 ± 0.03 and 0.32 ± 0.02 mM for the PC/PE/PS and PC/PE/PS/Ch vesicles, respectively (Figure 3B). These results are in correlation with the appearance of a half-maximal 11*R*-LOX activity (Figure 2 and Table 1). Also, in agreement with the catalytic activity measurements, the fluorescence energy transfer showed that 11*R*-LOX exhibits the highest Ca^{2+} affinity in the membrane docking reaction with PC/PE/anPL membranes, while with PC/anPL vesicles, the Ca^{2+} affinity of 11*R*-LOX remains remarkably lower (data not shown). In control experiments in the absence of Ca^{2+}, some increase in dansyl fluorescence was observed (Figure 3B), indicating that 11*R*-LOX–lipid binding occurs in the absence of Ca^{2+}. These binding events are clearly distinct from the appearance of activity. The presence of Ca^{2+} is absolutely essential for 11*R*-LOX activity.

Real-Time Kinetics of Ca^{2+}-Independent and Ca^{2+}-Dependent Docking of 11*R*-LOX to Different Lipid Mixtures. To further evaluate the Ca^{2+}-independent membrane insertion of 11*R*-LOX, we measured the kinetic traces in the presence of 0.1 mM EDTA (Figure 4A). For the Ca^{2+}-

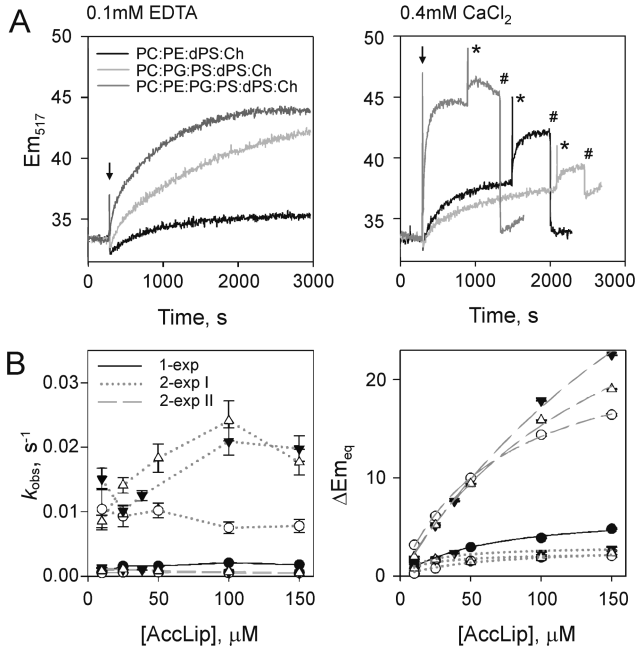

Figure 4. Kinetic analysis of docking of 11*R*-LOX to different phospholipid vesicles in the absence or presence of Ca^{2+}. (A) The docking was initiated by mixing 11*R*-LOX (↓, 250 nM) with indicated vesicles (50 μM AccLip) in 50 mM Tris-HCl (pH 8.0) and 100 mM NaCl at 20 °C in the presence of 0.1 mM EDTA or 0.4 mM $CaCl_2$. Shown are the additions of 0.6 mM $CaCl_2$ (*) and 2 mM EDTA (#). (B) Kinetic parameters for the Ca^{2+}-independent interaction between 11*R*-LOX (250 nM) and phospholipid vesicles with different compositions: (●) 35:40:5:20 PC:PE:dPS:Ch, (○) 50:10:15:5:20 PC:PG:PS:dPS:Ch, (▼) 10:40:25:5:20 PC:PE:PS:dPS:Ch, and (△) 10:40:10:15:5:20 PC:PE:PG:PS:dPS:Ch. The observed rate constants k_{obs} and ΔEm_{eq} were obtained by fitting of eq 5 (1-exp, black solid line) or eq 6 (2-exp, gray lines) to experimental traces. Experimental conditions: 50 mM Tris-HCl (pH 8.0), 100 mM NaCl, and 0.1 mM EDTA at 20 °C.

independent PC/PE/Ch vesicle–LOX interaction, all the time courses for different lipid concentrations can be fit to a single-exponential curve, yielding rate constants (k_{obs} = 0.0006–0.0021 s^{-1}) and ΔEm_{eq} values for each concentration of AccLip (Figure 4B). After addition of 30 mol % PI, PG, or PS to the vesicles (with or without PE), all the kinetic traces can be fit to a double-exponential curve. The binding curves show an initial,

dx.doi.org/10.1021/bi201690z | *Biochemistry* 2012, 51, 3310–3320

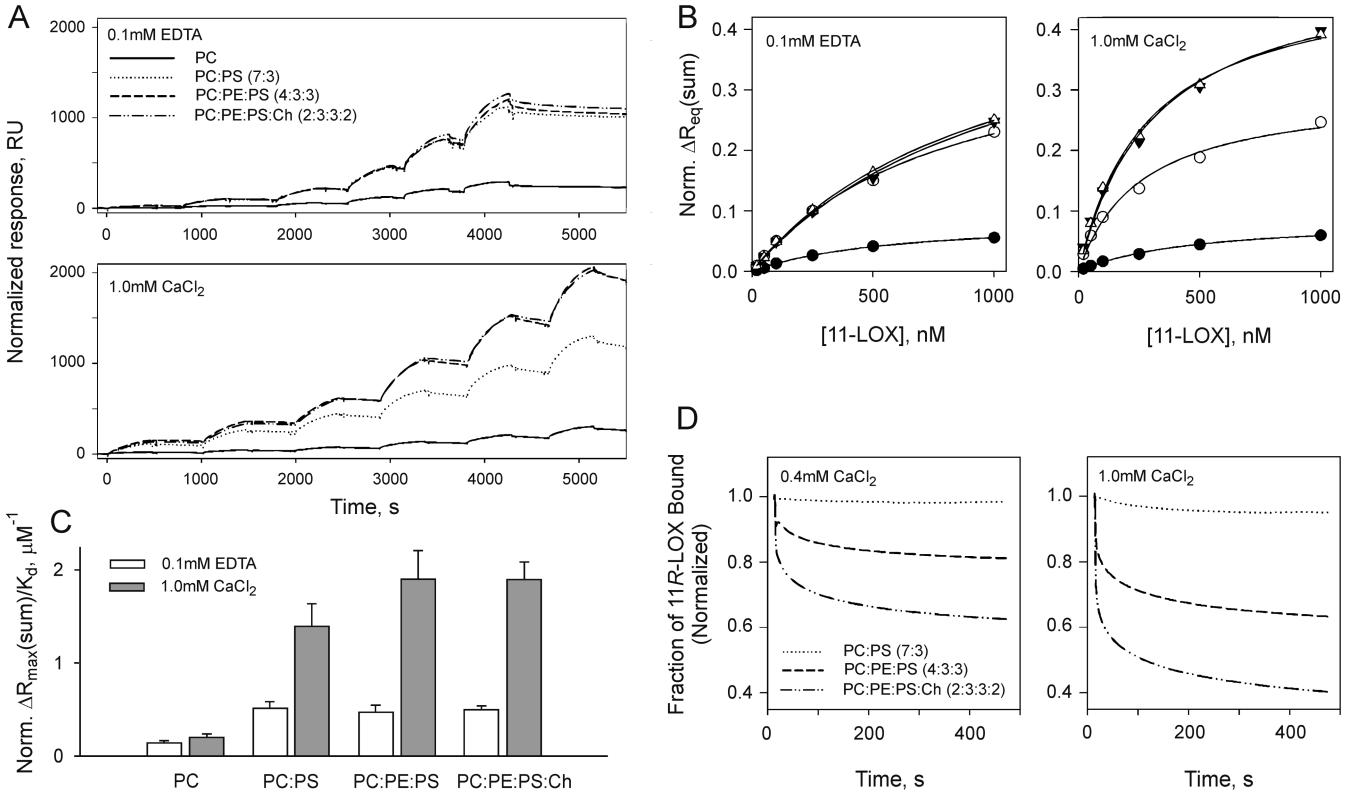

Figure 5. Kinetic and equilibrium SPR analyses of 11*R*-LOX−membrane binding. (A) Shown are SPR sensorgrams for the interaction between 11*R*-LOX and SUV using single-cycle kinetics. PC, PC/PS (7:3), PC/PE/PS (4:3:3), and PC/PE/PS/Ch (2:3:3:2) vesicles were immobilized on an L1 sensor chip, and various concentrations of 11*R*-LOX (20, 50, 100, 250, 500, and 1000 nM) were injected over the surface in the presence of 0.1 mM EDTA or 1.0 mM free $CaCl_2$. The response of the 11*R*-LOX interaction was normalized to the amount of SUV immobilized to the sensorchip. (B) Equilibrium binding of 11*R*-LOX to the sensorchip coated with PC (●), PC/PS (7:3, ○), PC/PE/PS (4:3:3, ▼), or PC/PE/PS/Ch (2:3:3:2, Δ) vesicles in the presence of 0.1 mM EDTA or 1.0 mM free $CaCl_2$. The binding isotherms were generated from the normalized $R_i + \Delta R_{eq1} + \Delta R_{eq2}$ from eq 6 [normΔR_{eq}(sum)] vs protein concentration. The solid line represents a theoretical curve obtained on the basis of normΔR_{max} and K_d values determined by the nonlinear least-squares analysis. (C) Efficiency of binding events. (D) Kinetics of dissociation of 11*R*-LOX upon removal of Ca^{2+}. 11*R*-LOX−Ca^{2+}−SUV ternary complexes were assessed on the sensorchip in the presence of 0.4 or 1.0 mM $CaCl_2$. The 11*R*-LOX dissociation was initiated by injection of 2 mM EDTA into the running buffer, which chelates the free Ca^{2+}. While no dissociation of 11*R*-LOX from the 11*R*-LOX−Ca^{2+}−PC complex was detected during the EDTA injection, this flow cell was used as a reference cell and subtracted out to eliminate refractive index changes due to a change in buffer.

faster increase in fluorescence (k_{obs1} = 0.007−0.024 s^{-1}) and a significantly slower (k_{obs2} = 0.0007−0.001 s^{-1}) second binding phase (Figure 4B, all data not shown). The observed rate constants for the Ca-independent membrane association are relatively independent of the lipid composition of vesicles and the concentration of accessible phospholipids, varying no more than ∼2-fold. There is no significant increase in emission intensity in the case of the fast binding phase (Figure 4B, 2-exp I). During the slow binding phase (Figure 4B, 2-exp II), a remarkable increase in ΔEm was achieved, while in the presence of PS, PG, or PI, ΔEm_{max2} was up to 10-fold larger than ΔEm_{max} in the absence of anPL (67 ± 11 and 6.6 ± 1.1 for the PC/PE/PS/Ch and PC/PE/Ch vesicles, respectively). The increase in ΔEm_{eq2} values with an increasing lipid concentration for PG-containing vesicles is comparable with that for PS-containing vesicles and is relatively independent of the presence of PE (Figure 4B).

In the presence of calcium, the observed rate constants and ΔEm values depend on the PE content of SUV. The addition of 11*R*-LOX to solutions containing PE/anPL liposomes and Ca^{2+} causes a fast skip of the emission intensity. The amplitude of the skip depends on the nature of the liposomes (Figure 4A, 0.4 mM $CaCl_2$). Generally, the Ca^{2+}-dependent membrane binding was found to be too fast to be analyzed. Addition of excess EDTA to the preformed ternary complex of protein, Ca^{2+}, and the vesicle caused the dissociation of the 11*R*-LOX−Ca^{2+}−SUV complex. The fluorescence intensities obtained for PE-containing vesicles returned to the baseline [Em_{517}(−Ca^{2+})], demonstrating that the binding is reversible (Figure 4A, 0.4 mM $CaCl_2$). For PC/PG/PS vesicles, the emission intensity did not return to that of the phospholipid alone. The extent of the decrease depends on the concentration of Ca^{2+} added previously, demonstrating that part of the binding observed with these vesicles at a present Ca^{2+} concentration was Ca^{2+}-independent.

Overall, the membrane interaction of 11*R*-LOX showed two distinct phases of association, with a fast initial phase followed by a second, slower phase. PC/PE/Ch vesicles did not show a significant energy transfer from protein added to the Ca-free solution. Anionic phospholipids [PI < PG ≈ PS (data not shown)] were essential for the Ca^{2+}-independent membrane binding of 11*R*-LOX. Interestingly, an analogous preference for anionic phospholipids appeared also by the modulation of 11*R*-LOX activity with different anPL levels (Figure 2A). The Ca^{2+}-dependent docking of 11*R*-LOX to lipid mixtures depends on the PE content. In the case of PC/PE/anPL liposomes, Ca^{2+}-

dx.doi.org/10.1021/bi201690z | *Biochemistry* 2012, 51, 3310−3320

mediated membrane binding occurs at lower concentrations of Ca^{2+} than with PC/anPL liposomes. In the absence of PE, at a lower Ca^{2+} concentration (<1 mM), the Ca^{2+}-independent nonproductive interaction of 11*R*-LOX with membranes is dominant. Therefore, the reaction of 11*R*-LOX with arachidonic acid coincided with and was likely driven by its Ca^{2+}-mediated membrane binding.

Direct Binding between 11*R*-LOX and SUV Detected by Surface Plasmon Resonance. SPR is dependent on the mass of protein bound to the membrane, while FRET is dependent on a number of parameters such as the molar concentration of the donor−acceptor pair, their distance, spectral overlaps, quantum yields, and orientation. To quantitatively assess the direct binding of 11*R*-LOX to vesicles, we subjected 11*R*-LOX to SPR analyses with the liposome-coated sensor chips. To follow the selectivity of 11*R*-LOX−SUV interactions, we tested the binding of 11*R*-LOX to PC, PC/PS, PC/PE/PS, and PC/PE/PS/Ch vesicles. As shown in Figure 5, the binding of 11*R*-LOX to the immobilized liposomes was concentration-dependent and nearly irreversible. In agreement with FRET data, the association phase data were fit well to a two-phase exponential equation, indicating that there are at least two essentially separate association−dissociation events occurring at the surface, one of which is approximately 1−2 orders of magnitude faster than the other ($k_{obs1} \sim 0.1-0.2\ s^{-1}$, and $k_{obs2} = 0.002-0.005\ s^{-1}$, respectively). The observed dissociation phase did not conform to a one-step or two-step interaction model. Therefore, association and dissociation rate constants could not be accurately determined in this study, and the normalized responses of two association events were summarized for equilibrium analysis.

In the absence of Ca^{2+}, 11*R*-LOX demonstrated a pronounced anionic lipid preference; i.e., there were ∼5 times as many binding sites on PS-containing vesicles as on PC vesicles (Figure 5 and Table 2). The addition of 30 mol % PE to the vesicles (i.e., PC/PE/PS or PC/PE/PS/Ch vesicles) did not influence the efficiency of the Ca^{2+}-independent membrane binding of 11*R*-LOX (Figure 5C). This is consistent with our vesicle binding data monitored via fluorescence (Figure 4) in which anionic phospholipids were essential for the Ca^{2+}-independent interaction of 11*R*-LOX with vesicles. Intriguingly, the binding response level for 11*R*-LOX was ∼2-fold lower in the presence of 0.4 mM $CaCl_2$ than without $CaCl_2$ in the buffer. Thus, it seems that there are different binding sites for the Ca^{2+}-independent and Ca^{2+}-dependent membrane binding of 11*R*-LOX, and the binding of Ca^{2+} would modify the Ca^{2+}-independent binding site(s) on 11*R*-LOX or the vesicle. Unlike the number of binding sites, the affinity of 11*R*-LOX for all the vesicles tested increased 2−5-fold in the presence of Ca^{2+}. The lipid composition of vesicles did not significantly influence K_d values. When PS was present in the vesicles [i.e., PC/PS (7:3) vesicles], the addition of 30 mol % PE caused an ∼2-fold increase in the number of binding sites for the Ca^{2+}-dependent interaction. Cholesterol did not have any significant effects on the efficiency of binding of 11*R*-LOX to immobilized vesicles.

To determine the reversibility of the Ca^{2+}-dependent membrane binding of 11*R*-LOX, the dissociation of the ternary complex of protein, Ca^{2+}, and immobilized vesicles upon removal of Ca^{2+} was monitored. Ternary 11*R*-LOX−Ca^{2+}−SUV complexes were created in the presence of 0.4 or 1.0 mM $CaCl_2$ (Figure 5D). The dissociation reaction was triggered by the injection of EDTA to chelate the free Ca^{2+}. No dissociation of 11*R*-LOX from the 11*R*-LOX−Ca^{2+}−PC complex was detected during the EDTA injection, and this flow cell was used as a reference cell. The dissociation of 11*R*-LOX from PC/PS vesicles was negligible (2−5%), indicating that under the conditions utilized in this study the binding of 11*R*-LOX to those vesicles was mostly Ca^{2+}-independent. A comparison of the time courses for dissociation of 11*R*-LOX from PC/PE/PS and PC/PE/PS/Ch vesicles revealed that the part of protein that dissociated from 11*R*-LOX−Ca^{2+}−liposome complexes accounted for 19 and 38%, respectively, when the complex was formed at 0.4 mM $CaCl_2$ and for 37 and 60%, respectively, when the complex was formed at 1.0 mM $CaCl_2$.

Together, these data further support the essential role of Ca^{2+} and PS binding in the membrane binding of 11*R*-LOX and an augmenting role of PE in the presence of Ca^{2+} and PS. PS and PE in the liposome affect the number of binding sites of 11*R*-LOX rather than its affinity for the membrane. 11*R*-LOX does interact with PC liposomes, but the number of binding sites remains very small. The addition of PS to liposome increases the efficiency of both Ca^{2+}-dependent and Ca-independent binding. PE in liposomes additionally enhances the Ca^{2+}-dependent binding but does not affect the Ca^{2+}-independent interaction of 11*R*-LOX with liposomes. PE and cholesterol in the vesicles have a considerable influence on the membrane binding mode of 11*R*-LOX.

Table 2. Kinetic Parameters of 11*R*-LOX with Immobilized SUV Monitored via SPR

	K_d (μM)	normΔR_{max}	n(AccLip/LOX)
	0.1 mM EDTA		
PC	0.59 ± 0.06	0.089 ± 0.004	570
PC/PS (7:3)	0.81 ± 0.10	0.41 ± 0.03	120
PC/PE/PS (4:3:3)	1.08 ± 0.15	0.51 ± 0.04	100
PC/PE/PS/Ch (2:3:3:2)	1.00 ± 0.07	0.50 ± 0.02	110
	0.4 mM $CaCl_2$		
PC	0.12 ± 0.02	0.055 ± 0.002	920
PC/PS (7:3)	0.15 ± 0.01	0.19 ± 0.03	270
PC/PE/PS (4:3:3)	0.16 ± 0.01	0.27 ± 0.01	180
PC/PE/PS/Ch (2:3:3:2)	0.15 ± 0.01	0.29 ± 0.01	200
	1.0 mM $CaCl_2$		
PC	0.39 ± 0.07	0.08 ± 0.01	650
PC/PS (7:3)	0.18 ± 0.03	0.25 ± 0.02	200
PC/PE/PS (4:3:3)	0.24 ± 0.04	0.44 ± 0.03	110
PC/PE/PS/Ch (2:3:3:2)	0.24 ± 0.02	0.45 ± 0.02	120
	2.0 mM $CaCl_2$		
PC	0.26 ± 0.05	0.08 ± 0.01	650
PC/PS (7:3)	0.13 ± 0.02	0.25 ± 0.02	200
PC/PE/PS (4:3:3)	0.12 ± 0.01	0.50 ± 0.01	100
PC/PE/PS/Ch (2:3:3:2)	0.13 ± 0.01	0.50 ± 0.02	110

DISCUSSION

This study provides the detailed kinetic description of a LOX on its interaction with lipids that helps in understanding the mechanism of membrane binding and activity regulation of lipoxygenases. Activation of LOX in the cells is achieved by a number of regulators, which can vary for individual enzymes.[3] Among those, Ca^{2+} is a common activator of LOX. Mutagenesis and X-ray diffraction studies have identified specific amino acids on 5-LOX,[9,29] 8*R*-LOX,[19] and the reticulocyte-type 15-

dx.doi.org/10.1021/bi201690z | *Biochemistry* 2012, 51, 3310−3320

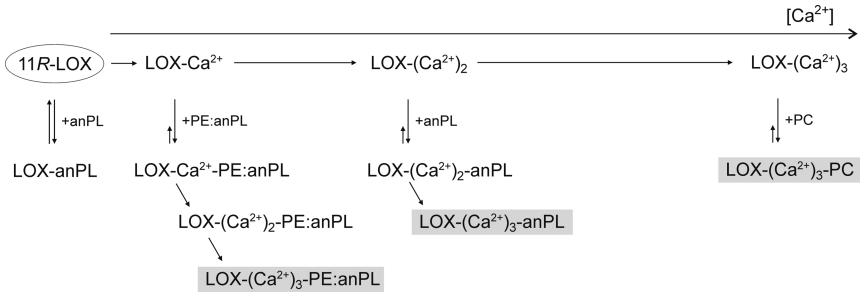

Figure 6. Proposed mechanism for membrane binding and Ca^{2+} activation of 11*R*-LOX in the presence of different model membranes. Fully active 11*R*-LOX−Ca^{2+}−SUV ternary complexes are highlighted.

LOX[11,12] that are involved in Ca^{2+} and membrane binding, but the mechanism of how Ca^{2+} affects LOX membrane binding and catalysis has remained unclear.

11*R*-LOX has a low Ca^{2+} affinity and requires non-physiologically high calcium concentrations for membrane binding and activation.[36] We investigated the Ca^{2+}-dependent and -independent interaction of 11*R*-LOX with liposomes and the modulation of the membrane binding of the enzyme by changes in the lipid environment. These data show that the nature of the model membrane can greatly enhance the Ca^{2+} and membrane binding properties of 11*R*-LOX; i.e., the high content of anPL and PE in the model membrane is essential for achieving effective and productive Ca^{2+}-dependent membrane binding of 11*R*-LOX. Figure 6 summarizes significant findings and the proposed mechanism for 11*R*-LOX membrane binding and activation.

The biphasic binding kinetics observed in FRET and SPR experiments suggests that the interaction of 11*R*-LOX with phospholipid surfaces is complex. Whereas a similar behavior is equally inherent in the Ca^{2+}-independent and -dependent interactions of 11*R*-LOX and is not considerably influenced by the nature of vesicles, it is the merit of the protein itself rather than induced by the membrane surface. The two-step association phase could result from the protein colliding with the surface in multiple orientations, binding weakly, and then reorienting or could be explained by the existence of different conformational states of the protein. These states may exist in the absence of ligand or be induced by its binding.[40] On the other hand, lipoxygenases are composed of two domains, and both of them could be implicated in membrane binding.[11,14] Therefore, the biphasic binding kinetics observed might also be due to the fact that there are two constitutive binding sites for membrane association in 11*R*-LOX.

When the Ca^{2+} dependence for the activation of 11*R*-LOX was studied in the presence of different model membranes, it was observed that 11*R*-LOX responded differently to increasing concentrations of Ca^{2+} when vesicles of different compositions were used (Figure 2 and Table 1). The tested vesicles did not induce the activation of 11*R*-LOX at Ca^{2+} concentrations of <10 μM. These data suggest a molecular mechanism in which 11*R*-LOX (membrane-bound or not) binds a single Ca^{2+} prior to associating with another Ca^{2+} and a phospholipid headgroup. In our experiments, the presence of PE weakened the need of 11*R*-LOX for Ca^{2+} at lower concentrations of Ca^{2+} rather than the presence of anionic phospholipids, suggesting that 11*R*-LOX exhibits different binding motifs for PE and anPL and that PE and anPL increase the Ca^{2+} binding affinity of different binding sites. On the basis of the primary structure homology of 11*R*-LOX and *P. homomalla* 8*R*-LOX,[19] we propose that 11*R*-LOX has three Ca^{2+}-binding sites in its C2-like domain. In the absence of PE, at least two of them have to be occupied before the productive membrane binding of the enzyme could occur (Figure 6). The presence of anionic phospholipids enhances the Ca^{2+} binding affinity in the third binding site. The addition of PE to vesicles enhances the 11*R*-LOX activity at lower concentrations of Ca^{2+}, indicating the influence of the PE headgroup(s) in the second Ca^{2+} binding site (Figure 6). The binding of the second Ca^{2+} and one or more PE headgroups would not facilitate the subsequent binding of the third Ca^{2+} except in the presence of anionic phospholipids (Figure 2). In the absence of anPL and PE in the membranes, three Ca^{2+} ions must first bind to 11*R*-LOX before it docks to the membrane surface (Figure 6). Without the synergistic effects of PE and anPL, the binding of the second and third Ca^{2+} would exhibit a low affinity and a minimal positive cooperativity. Submillimolar Ca^{2+} concentrations are unable to drive the productive docking of 11*R*-LOX to the membranes lacking PE and anPL.

In summary, on the basis of protein−lipid interactions, the TAMA mechanism is proposed to drive the targeting of 11*R*-LOX to the specific membranes. From the data reported here, we suppose a mechanism by which 11*R*-LOX binds to membranes via two distinct modes of interaction. Early in the assembly pathway, Ca^{2+}-independent interactions mediated by the N-terminal C2-like domain and catalytic domain of 11*R*-LOX and anionic phospholipids might clamp the 11*R*-LOX−membrane complex. Following the influx of Ca^{2+}, 11*R*-LOX penetrates the membranes and drives the final assembly of the complex, or changes the orientation relative to the plane of the lipid bilayer, to trigger the accessibility to the active site of the enzyme. Regardless of the state of 11*R*-LOX, its Ca^{2+}-triggered activation seems to be regulated through interactions with PE and anPL headgroups.

To date, no detailed analysis of the effect of lipid composition on membrane binding efficiency, Ca^{2+} affinity, and catalytic activity has been conducted with any other LOX. However, studies of Ca^{2+}-induced binding of 5-LOX to PC membranes showed that 5-LOX binds Ca^{2+} in a reversible manner with the stoichiometry of maximal binding around two Ca^{2+} ions per enzyme.[3,9,15] It is suggested that the PC selectivity directs 5-LOX to the nuclear envelope.[10,29] Negatively charged lipids added to PC vesicles inhibit 5-LOX, but a cationic lipid is more stimulatory than PC alone. Although binding to cationic membranes is Ca^{2+}-independent, Ca^{2+} is required for 5-LOX activity.[30]

The comparison of activation of 11*R*- and 5-LOX reveals some parallels between these two enzymes that might serve as general mechanistic principles of activation of Ca^{2+}- and membrane-dependent LOX. Lipoxygenases can bind to

membranes in productive or nonproductive modes, and membrane binding per se might not confer LOX activity. Ca^{2+} binding with consecutive conformational changes is a prerequisite for productive membrane association. In living cells, distinct membrane phospholipids characteristic of a specific LOX selectively bind and direct the enzyme to proper membranes or organelles.

AUTHOR INFORMATION

Corresponding Author

*E-mail: nigulas.samel@ttu.ee. Telephone: 372-620-4376. Fax: 372-670-3683.

Funding

This reseach was supported by Estonian Science Foundation Grants 8276 (to I.J.), 8300 (to A.L.), and 7556 (to R.K.) and the Estonian Ministry of Education and Research (a grant to N.S.).

Notes

The authors declare no competing financial interest.

ABBREVIATIONS

LOX, lipoxygenase; $cPLA_2$, cytosolic phospholipase A_2; PC, phosphatidylcholine; PE, phosphatidylethanolamine; PS, phosphatidylserine; PI, phosphatidylinositol; PG, phosphatidylglycerol; Ch, cholesterol; dPS, dansylPS or 1,2-dioleyl-*sn*-glycero-3-phospho-L-serine-*N*-(5-dimethylamino-1-naphthalenesulfonyl); SUV, small unilamellar vesicles; anPL, anionic phospholipids; AccLip, accessible phospholipid; PM, plasma membrane; NM, nuclear membrane; AA, arachidonic acid; FRET, fluorescence resonance energy transfer; SPR, surface plasmon resonance; TAMA, target-activated-messenger-affinity.

REFERENCES

(1) Ivanov, I., Heydeck, D., Hofheinz, K., Roffeis, J., O'Donnell, V. B., Kuhn, H., and Walther, M. (2010) Molecular enzymology of lipoxygenases. *Arch. Biochem. Biophys. 503*, 161−174.

(2) Schneider, C., Pratt, D. A., Porter, N. A., and Brash, A. R. (2007) Control of oxygenation in lipoxygenase and cyclooxygenase catalysis. *Chem. Biol. 14*, 473−488.

(3) Radmark, O., and Samuelsson, B. (2010) Regulation of the activity of 5-lipoxygenase, a key enzyme in leukotriene biosynthesis. *Biochem. Biophys. Res. Commun. 396*, 105−110.

(4) Dobrian, A. D., Lieb, D. C., Cole, B. K., Taylor-Fishwick, D. A., Chakrabarti, S. K., and Nadler, J. L. (2011) Functional and pathological roles of the 12- and 15-lipoxygenases. *Prog. Lipid Res. 50*, 115−131.

(5) Gilbert, N. C., Bartlett, S. G., Waight, M. T., Neau, D. B., Boeglin, W. E., Brash, A. R., and Newcomer, M. E. (2011) The structure of human 5-lipoxygenase. *Science 331*, 217−219.

(6) Jankun, J., Doerks, T., Aleem, A. M., Lysiak-Szydlowska, W., and Skrzypczak-Jankun, E. (2008) Do human lipoxygenases have a PDZ regulatory domain? *Curr. Mol. Med. 8*, 768−773.

(7) Chahinian, H., Sias, B., and Carriere, F. (2000) The C-terminal domain of pancreatic lipase: Functional and structural analogies with c2 domains. *Curr. Protein Pept. Sci. 1*, 91−103.

(8) Allard, J. B., and Brock, T. G. (2005) Structural organization of the regulatory domain of human 5-lipoxygenase. *Curr. Protein Pept. Sci. 6*, 125−131.

(9) Hammarberg, T., Provost, P., Persson, B., and Radmark, O. (2000) The N-terminal domain of 5-lipoxygenase binds calcium and mediates calcium stimulation of enzyme activity. *J. Biol. Chem. 275*, 38787−38793.

(10) Chen, X. S., and Funk, C. D. (2001) The N-terminal "β-barrel" domain of 5-lipoxygenase is essential for nuclear membrane translocation. *J. Biol. Chem. 276*, 811−818.

(11) Walther, M., Anton, M., Wiedmann, M., Fletterick, R., and Kuhn, H. (2002) The N-terminal domain of the reticulocyte-type 15-lipoxygenase is not essential for enzymatic activity but contains determinants for membrane binding. *J. Biol. Chem. 277*, 27360−27366.

(12) Walther, M., Wiesner, R., and Kuhn, H. (2004) Investigations into calcium-dependent membrane association of 15-lipoxygenase-1. Mechanistic roles of surface-exposed hydrophobic amino acids and calcium. *J. Biol. Chem. 279*, 3717−3725.

(13) Aleem, A. M., Jankun, J., Dignam, J. D., Walther, M., Kühn, H., Svergun, D. I., and Skrzypczak-Jankun, E. (2008) Human platelet 12-lipoxygenase, new findings about its activity, membrane binding and low-resolution structure. *J. Mol. Biol. 376*, 193−209.

(14) Maccarrone, M., Salucci, M. L., van Zadelhoff, G., Malatesta, F., Veldink, G., Vliegenthart, J. F., and Finazzi-Agro, A. (2001) Tryptic digestion of soybean lipoxygenase-1 generates a 60 kDa fragment with improved activity and membrane binding ability. *Biochemistry 40*, 6819−6827.

(15) Rouzer, C. A., and Samuelsson, B. (1985) On the nature of the 5-lipoxygenase reaction in human leukocytes: Enzyme purification and requirement for multiple stimulatory factors. *Proc. Natl. Acad. Sci. U.S.A. 82*, 6040−6044.

(16) Koljak, R., Boutaud, O., Shieh, B.-H., Samel, N., and Brash, A. R. (1997) Identification of a naturally occurring peroxidase-lipoxygenase fusion protein. *Science 277*, 1994−1996.

(17) Boutaud, O., and Brash, A. R. (1999) Purification and catalytic activities of the two domains of the allene oxide synthase-lipoxygenase fusion protein of the coral *Plexaura homomalla*. *J. Biol. Chem. 274*, 33764−33770.

(18) Lõhelaid, H., Järving, R., Valmsen, K., Varvas, K., Kreen, M., Järving, I., and Samel, N. (2008) Identification of a functional allene oxide synthase-lipoxygenase fusion protein in the soft coral *Gersemia fruticosa* suggests the generality of this pathway in octocorals. *Biochim. Biophys. Acta 1780*, 315−321.

(19) Oldham, M. L., Brash, A. R., and Newcomer, M. E. (2005) Insights from the X-ray crystal structure of coral 8R-lipoxygenase: Calcium activation via a C2-like domain and a structural basis of product chirality. *J. Biol. Chem. 280*, 39545−39552.

(20) Tatulian, S. A., Steczko, J., and Minor, W. (1998) Uncovering a calcium-regulated membrane-binding mechanism for soybean lipoxygenase-1. *Biochemistry 37*, 15481−15490.

(21) Leventis, P. A., and Grinstein, S. (2010) The distribution and function of phosphatidylserine in cellular membranes. *Annu. Rev. Biophys. 39*, 407−427.

(22) van Meer, G., and de Kroon, A. I. (2011) Lipid map of the mammalian cell. *J. Cell Sci. 124*, 5−8.

(23) Vance, J. E. (2008) Phosphatidylserine and phosphatidylethanolamine in mammalian cells: Two metabolically related aminophospholipids. *J. Lipid Res. 49*, 1377−1387.

(24) Imbs, A. B., Demina, O. A., and Demidkova, D. A. (2006) Lipid class and fatty acid composition of the boreal soft coral *Gersemia rubiformis*. *Lipids 41*, 721−725.

(25) Nalefski, E. A., Wisner, M. A., Chen, J. Z., Sprang, S. R., Fukuda, M., Mikoshiba, K., and Falke, J. J. (2001) C2 domains from different Ca^{2+} signaling pathways display functional and mechanistic diversity. *Biochemistry 40*, 3089−3100.

(26) Cho, W., and Stahelin, R. V. (2006) Membrane binding and subcellular targeting of C2 domains. *Biochim. Biophys. Acta 1761*, 838−849.

(27) Lemmon, M. A. (2008) Membrane recognition by phospholipid-binding domains. *Nat. Rev. Mol. Cell Biol. 9*, 99−111.

(28) Manna, D., Bhardwaj, N., Vora, M. S., Stahelin, R. V., Lu, H., and Cho, W. (2008) Differential roles of phosphatidylserine, PtdIns(4,5)P2, and PtdIns(3,4,5)P3 in plasma membrane targeting of C2 domains. Molecular dynamics simulation, membrane binding, and cell translocation studies of the PKCα C2 domain. *J. Biol. Chem. 283*, 26047−26058.

(29) Kulkarni, S., Das, S., Funk, C. D., Murray, D., and Cho, W. (2002) Molecular basis of the specific subcellular localization of the C2-like domain of 5-lipoxygenase. *J. Biol. Chem. 277*, 13167−13174.

(30) Pande, A. H., Moe, D., Nemec, K. N., Qin, S., Tan, S., and Tatulian, S. A. (2004) Modulation of human 5-lipoxygenase activity by membrane lipids. *Biochemistry 43*, 14653−14666.
(31) Andersson, E., Schain, F., Svedling, M., Claesson, H.-E., and Forsell, P. K. (2006) Interaction of human 15-lipoxygenase-1 with phosphatidylinositol bisphosphates results in increased enzyme activity. *Biochim. Biophys. Acta 1761*, 1498−1505.
(32) Corbin, J. A., Evans, J. H., Landgraf, K. E., and Falke, J. J. (2007) Mechanism of specific membrane targeting by C2 domains: Localized pools of target lipids enhance Ca^{2+} affinity. *Biochemistry 46*, 4322−4336.
(33) Guerrero-Valero, M., Marin-Vicente, C., Gomez-Fernandez, J. C., and Corbalan-Garcia, S. (2007) The C2 domains of classical PKCs are specific PtdIns(4,5)P2-sensing domains with different affinities for membrane binding. *J. Mol. Biol. 371*, 608−621.
(34) Li, L., Shin, O.-H., Rhee, J.-S., Arac, D., Rah, J.-C., Rizo, J., Südhof, T., and Rosenmund, C. (2006) Phosphatidylinositol phosphates as co-activators of Ca^{2+} binding to C2 domains of synaptotagmin 1. *J. Biol. Chem. 281*, 15845−15852.
(35) Montaville, P., Coudevylle, N., Radhakrishnan, A., Leonov, A., Zweckstetter, M., and Becker, S. (2008) The PIP2 binding mode of the C2 domains of rabphilin-3A. *Protein Sci. 17*, 1025−1034.
(36) Mortimer, M., Järving, R., Brash, A. R., Samel, N., and Järving, I. (2006) Identification and characterization of an arachidonate 11R-lipoxygenase. *Arch. Biochem. Biophys. 445*, 147−155.
(37) Haining, J. L., and Axelrod, B. (1958) Induction period in the lipoxidase-catalyzed oxidation of linoleic acid and its abolition by substrate peroxide. *J. Biol. Chem. 232*, 193−202.
(38) Zheng, Y., and Brash, A. R. (2010) Dioxygenase activity of epidermal lipoxygenase-3 unveiled: Typical and atypical features of its catalytic activity with natural and synthetic polyunsaturated fatty acids. *J. Biol. Chem. 285*, 39866−39875.
(39) Zheng, Y., and Brash, A. R. (2010) On the role of molecular oxygen in lipoxygenase activation: Comparison and contrast of epidermal lipoxygenase-3 with soybean lipoxygenase-1. *J. Biol. Chem. 285*, 39876−39887.
(40) Prinz, H (2010) Hill coefficients, dose-response curves and allosteric mechanisms. *J. Chem. Biol. 3*, 37−44.